Structural-Parametric Optimization of Strip Protection Devices Based on Generative Template Representation

Alena Krasnoperova
Television and Control Department
Tomsk State University of Control Systems and Radioelectronics
Tomsk, Russian Federation
alena.s.krasnoperova@tusur.ru

Anton Belousov
Television and Control Department
Tomsk State University of Control Systems and Radioelectronics
Tomsk, Russian Federation
anton.o.belousov@tusur.ru

***Abstract*—This paper proposes a novel approach to the automated design of multiconductor strip modal filters (MFs), based on generative template representation and structural-parametric optimization. The optimization was performed using the Latin hypercube sampling (LHS) algorithm according to two criteria: minimizing the maximum interference voltage level (U_{out}) at the MF output and matching the MF to a 50 Ω transmission path (equating the input voltage U_{in} to half the EMF). We considered two formulations of the objective function (OF) and their respective normalization coefficients. Consequently, two optimization strategies were proposed. Strategy 1 executes a direct search for the best MF topology followed by local refinement. Strategy 2 employs a sequential selection of the most promising topologies, dynamically narrowing the search space until the global best is identified. The results demonstrated that strategy 2 effectively bypasses local extrema and allocates computational resources more efficiently. As a result of optimizing 14 unique topologies, strategy 1 converged to U_{out}=46 mV at U_{in}=500 mV, whereas strategy 2 outperformed it, yielding U_{out}=37 mV (a 19.5% improvement) at U_{in}=501 mV. Furthermore, the best-synthesized topologies were found to correspond to MFs with broad-side coupling, which maximized the difference in per-unit-length mode delays of the decomposition pulses. Finally, we outline future development trajectories for the proposed automated design strategies.**

Keywords*—*electromagnetic compatibility, modal filters, ultrashort pulses, structural-parametric optimization, generative synthesis.

I. Introduction

Modern radio-electronic equipment (REE) faces increasingly stringent requirements for ensuring electromagnetic compatibility (EMC). This is driven by the growing complexity of the electromagnetic environment caused by the widespread deployment of REE, its increased placement density, and the growing availability of powerful sources of electromagnetic interference [1], [2]. EMC violations lead to degradation of REE performance, malfunctions, and disruptions in operating modes, and, in some cases, complete REE failure. This is particularly critical for information transmission and processing systems, where high operational reliability is required.

Related to sources of intentional electromagnetic interference (IEMI), conducted interference that propagates through interconnects is considered the most hazardous. Unlike radiated interference, conducted disturbances are injected directly into REE circuits without undergoing significant attenuation from shielding. Consequently, they can affect sensitive REE components across the entire length of power supply and signal transmission lines [3].

Among others, ultrawideband (UWB) interference poses a significant threat to REE, with ultrashort pulses (USPs) being a specific type [4], [5]. The absorbed energy of a USP is localized and, due to the short pulse duration, does not dissipate to the surrounding REE components. This contributes to defect formation in sensitive heat dissipation zones [6] and disrupts the REE operating mode. The response time of traditional protection devices (e.g., TVS diodes or varistors) significantly exceeds the USP duration. Consequently, a substantial portion of the pulse interference energy reaches the protected circuits [7]. One solution to this problem is structures based on modal phenomena, specifically modal filters (MFs). These devices decompose the exciting USP into a sequence of pulses with smaller amplitudes because of the difference in per-unit-length mode delays in the transmission line [8], [9].

While numerous studies have extensively analyzed MF characteristics across various strip and cable configurations, investigating electrophysical parameter influences and the emergence of additional pulses [10], [11], the robust structural synthesis of MFs remains a critical bottleneck. The conventional approach relies heavily on the parametric optimization of a pre-selected, fixed geometry, lacking the capacity to generalize across an arbitrary class of topologies.

Currently, the MF design process is largely heuristic and iterative. It relies on a manual combination of topological and circuit selection (directed structural synthesis) followed by parametric optimization (directed parametric synthesis). Initially, a base configuration is simulated for a specific task. If the calculated characteristics fail to satisfy the requirements, the topology is manually modified, or its parameters are heavily subjected to global optimization algorithms. This creates a computationally expensive loop of empirical structural-parametric optimization, where the search strategy and feasible solution space are constantly readjusted based on intermediate results [12].

Fundamentally, MF parametric optimization suffers from dimensionality. It involves a vast array of variable geometric and electrophysical parameters and exhibits highly nonlinear

The reported study was funded by the Ministry of Science and Higher Education of the Russian Federation (Project FEWM-2024-0005).

characteristic dependencies. Specifically, the relative positioning of conductors, their dimensions, and material properties exert a severe influence on performance. Under these conditions, an exhaustive grid search is practically impossible, and classical local optimization methods incur prohibitive computational costs. To circumvent this, global optimization method, particularly evolutionary algorithms, are widely deployed to handle the multicriteria nature of the problem and navigate multiple local extrema [13]. Nevertheless, expanding this formalization to analyze multiple disparate structures simultaneously remains non-trivial and computationally explosive, severely limiting its practical utility.

A highly promising solution is automated generative synthesis based on parametric template representation. In this framework, novel configurations (i.e., varying topologies) are generated through the directed variation of parameters and the dynamic modification of templates that bound the feasible topological space. This automates the search process, intrinsically respects physical and manufacturing constraints, and strategically narrows the search space toward the most promising regions without sacrificing solution quality.

However, this generative approach remains computationally demanding. Classical algorithms are prone to premature convergence in local extrema or require unacceptable execution times. This dictates the urgent need for multi-stage search strategies designed to discard unpromising templates at early stages, thereby reallocating computational resources to viable candidates. Therefore, the primary purpose of this study is to develop and comparatively analyze advanced search strategies for the multicriteria structural-parametric optimization of strip MFs based on automated generative template representation.

II. Optimization Approaches

To calculate the characteristics and perform the optimization, we used the TUSUR EMC simulation environment (formerly TALGAT) [14] and assumed that *T*-waves were propagating within the MFs. The initial simulation step generated two-dimensional geometric models of the structures to calculate the per-unit-length electrostatic (**C**) and electromagnetic (**L**) induction matrices. To consider losses, we computed the per-unit-length conductivity (**G**) and resistance (**R**) matrices. From these primary parameters, we derived the secondary characteristics: the characteristic impedance matrices ($\mathbf{Z}_C$) and per-unit-length mode delays (τ_i).

The strip MFs were optimized using the Latin hypercube sampling (LHS) algorithm in Python. This method ensures a uniform distribution of pseudorandom points across the multidimensional parameter space [15].

The optimization relied on a two-criterion objective function (OF) and incorporated an amplitude criterion and a matching criterion. The former minimizes the maximum voltage level at the MF output $U_{out}(t)$. The latter minimizes the reflections of useful high-frequency signals at the MF input by equating the input voltage $U_{in}(t)$ to half the source EMF $E(t)$.

The initial multicriteria OF formulation reduces both criteria to a minimization task [16]. To simultaneously address them, we defined the OF as a sum of weighted, normalized criteria:

$$F_1 = M_1 \frac{\max(U_{out}(t))}{\max(E(t))} + M_2 \frac{|\max(E(t)) - 2\max(U_{in}(t))|}{\max|E(t)|}, \quad (1)$$

where M_i are weight coefficients equal to 0.5.

Although widely used, OF (1) inherently permits mutual criteria compensation. It means that the degradation of one criterion can be mathematically offset by the improvement of the other. To prevent this, we introduced a second multicriteria OF formulation using a least-squares sum of the weighted normalized criteria. This approach effectively penalizes the criterion with the larger deviation, thereby eliminating such compensation. Additionally, we revised the normalization approach for the individual criteria. In OF (1), dividing by the theoretical maximum $E(t)$ makes the amplitude criterion numerically much smaller than the matching criterion, which distorts the optimization priority. To balance this, OF (2) introduces empirical normalization coefficients:

$$F_2 = \sqrt{M_1 \left(\frac{\max(U_{out}(t))}{K_1} \right)^2 + M_2 \left(\frac{\max(E(t)) - 2\max(U_{in}(t))}{K_2} \right)^2}, \quad (2)$$

where K_i are the new normalization coefficients. The M_i values are also equal to 0.5.

K_1 and K_2 were derived from a preliminary global search using OF (1). K_1 represents the maximum observed error of the amplitude criterion, and K_2 represents the maximum error of the matching criterion. The computed values were K_1=0.25 and K_2=0.64.

To evaluate the stability across a series of runs, we calculated the deviation Δ as follows:

$$\Delta = \left| \frac{X_1 - X_2}{X_1 + X_2} \right| \cdot 100\%, \quad (3)$$

where X_1 and X_2 are the maximum and minimum observed values.

Our study focused on multiconductor strip MFs with three signal conductors. Fig. 1 illustrates the cross sections of the investigated MFs. For a systematic analysis, three baseline structural classes were distinguished: configurations with edge coupling and either an infinite ground plane (MF 1) or a reference conductor (MF 2), and configurations with broad-side coupling and a single reference conductor (MF 3), which are derived using automated generative synthesis. The algorithm automatically synthesizes various cross-sectional topologies, supporting both edge coupling (on a single substrate side) and broad-side coupling (across opposite substrate sides).

The geometric models of the MFs are represented as a set of discrete positions (slots) for potential conductor placement. The cross section of MF 1 is depicted in Fig. 1*a*, where the signal conductors occupy slots 1–3 above the ground plane, whereas MF 2 is shown in Fig. 1*b* (with slot 4 assigned to the reference conductor). The geometric model of MF 3 features six discrete slots for potential conductor placement (Fig. 1*c*). During the generative synthesis, the algorithm iteratively assigns each slot the status of either a signal (active A or passive P) or a reference (R) conductor. Any slots not utilized in the placement remain vacant.

A defining constraint of the synthesized topologies (Fig. 1*c*) is the mandatory formation of broad-side electromagnetic coupling. We enforced this by requiring at least one vertically aligned conductor pair (slots 1/4, 2/5, or 3/6). The active conductor is strictly assigned to the upper slot of this pair. The positions for the remaining passive and reference conductors are populated via an exhaustive combinatorial search across the available slots. Consequently, the synthesis yields one geometric model for MF 1, three models for MF 2 (varying the reference conductor position), and ten models for MF 3 (constrained to exactly three signal conductors). For identification, the 14 generated MF topologies were assigned letter designations (ID), which are detailed in Table I.

TABLE I. POSITIONS OF SIGNAL CONDUCTORS (A AND P) AND GROUND (PLANE, R) IN MF 1–3 TOPOLOGIES

MF ID	MF	Discrete position					
		1	2	3	4	5	6
A	1	A	P	P	Ground plane		
B	2	A	R	P	P		
C	2	A	P	R	P		
D	2	A	P	P	R		
E	3	A	R	P	P		
F	3	A			P	R	P
G	3	A	P	R	P		
H	3	A			P	P	R
I	3	P	A	R		P	
J	3		A	R	P	P	
K	3	P	A			P	R
L	3		A		P	P	R
M	3	P	R	A			P
N	3			A	P	R	P

The geometric models of the cross sections in Fig. 1 are defined by the conductor width (w) and thickness (t), the gaps between them (s_i), the substrate thickness (h), and the offset from the outer conductors to the MF edges (d). We optimized the parameters that directly govern the output voltage waveform within the following boundaries: 100–2000 μm for h, 18–200 μm for t, and 100–2000 μm for s_i. The remaining parameters were fixed to standard PCB values: w=1000 μm, d=3w, substrate relative permittivity ε_r=4.5, and the dielectric loss tangent tanδ=0.025.

All MFs (14 topologies) operate as 3-conductor transmission lines; their equivalent circuit is shown in Fig. 2. The MF lengths were set to l=60 cm, and the resistances at the ends of all conductors (R_G, R_L, and R) were 50 Ω. The parameters of the exciting USP were as follows: an EMF amplitude of 1 V; rise, fall, and flat top durations of 50 ps each; and a total pulse duration of 150 ps.

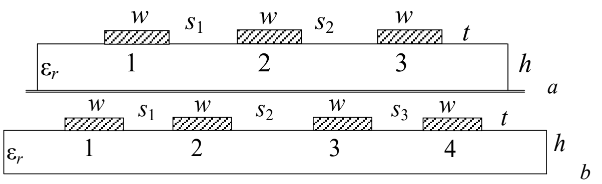

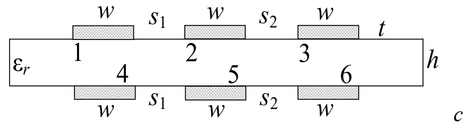

Fig. 1. Cross sections of MF 1 (*a*), 2 (*b*), and 3 (*c*).

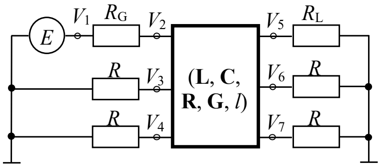

Fig. 2. Equivalent circuit of MFs 1–3.

We proposed and compared two structural-parametric optimization strategies (block diagrams in Fig. 3). Strategy 1 relies on OF F_1. It executes a direct global search for the best geometry using 80% of the total number of computations (N_{it}), reserving the remaining 20% to refine the best found topology (Fig. 3*a*). However, the normalization type of OF F_1, the fixed ranges of the optimized parameters, and the expenditure of N_{it} on unpromising MF topologies necessitated the development of strategy 2.

Strategy 2 utilizes OF F_2 and implements a sequential tournament selection algorithm. Here, the N_{it} value is distributed among three calculation stages in a 50%, 25%, and 25% ratio. Unlike strategy 1, this approach involves sorting and discarding the inferior topologies (from 14 to 7, and then to the 3 best ones). Crucially, it dynamically narrows the parameter search space (by ±50% and ±25%) around the local optima of the best topologies (Fig. 3*b*).

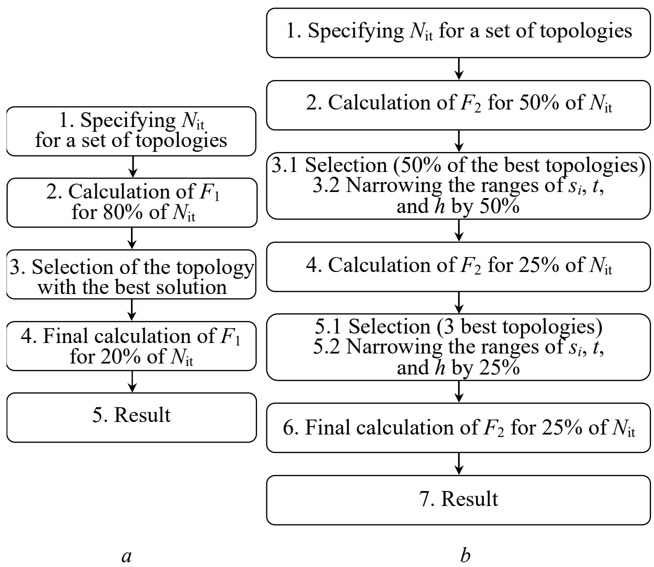

Fig. 3. Base strategies 1 (*a*) and 2 (*b*) for the MF structural-parametric optimizations.

III. OPTIMIZATION RESULTS

The calculation results for strategies 1 and 2 are presented in Table II and Table III, respectively, where № denotes the run number. For analytical convenience, the letter designations corresponding to Table I are compiled in the “MF ID” column.

TABLE II. MF OPTIMIZATION RESULTS FOR STRATEGY 1

№	MF ID	t, µm	h, µm	s_1, µm	s_2, µm	U_{in}, mV	U_{out}, mV
N_{it}=500							
1	F	42.0	177.6	354.2	576.4	515	56
2	H	39.4	176.3	111.6	953.4	510	46
3	K	56.3	172.4	206.3	1168.5	495	71
4	N	32.8	103.0	1796.4	771.4	504	61
5	I	19.7	106.3	957.5	1478.2	503	78
Δ, %		48.2	26.6	88.30	43.9	1.96	25.8
N_{it}=1000							
1	F	38.3	118.8	893.0	1239.3	515	58
2	K	20.5	145.1	260.8	1772.1	503	55
3	K	67.1	208.1	287.9	1951.4	517	71
4	I	67.4	208.8	163.4	1034.3	497	76
5	F	26.7	105.4	490.2	502.8	499	69
Δ, %		53.4	32.9	69.1	55.8	1.96	16.0
N_{it}=2500							
1	F	29.2	105.2	915.6	1555.8	510	49
2	M	33.0	101.3	1872.6	667.4	500	69
3	E	47.5	147.2	362.9	500.9	502	64
4	G	62.9	195	110.5	1065.6	500	55
5	**J**	**21.6**	**184.7**	**147.3**	**809.4**	**500**	**46**
Δ, %		48.9	31.6	88.9	51.3	1.0	20.0

Strategy 1 converged exclusively to MF 3 topological variants. Table II exposes inherent inconsistency of strategy 1, meaning that across all N_{it} values, the results converge to different topologies depending on the initial random LHS sample. This confirms the assumption that due to the strict selection of a single best option at step 3 (Fig. 3*a*) and the absence of sequential narrowing of the optimized parameter ranges, LHS continues to explore the entire parameter space. Consequently, the probability of reaching the global extremum is low, resulting in highly erratic repeatability.

Assuming equal criteria weights (0.5/0.5), strategy 1 achieved its best result at N_{it}=2500 (run 5, MF J). This topology perfectly matched the line (U_{in}=500 mV, half of $E(t)$) while yielding the lowest output USP amplitude (U_{out}=46 mV). At the same time, run 2 at N_{it}=500 (MF H) achieved a similar interference suppression but failed the matching criterion (U_{in}=510 mV). This severe dispersion proves that simply inflating the iteration count without dynamically narrowing the search boundaries does not guarantee a systematic improvement in the results when using strategy 1.

The analyses of deviation Δ in strategy 1 reveals a severe lack of parameter convergence. As N_{it} increases, the range of optimized parameters remains high: the deviations of s_1 and s_2 at N_{it}=2500 reach 88.9% and 51.3%, while those for t and h reach 48.9% and 31.6%, respectively. Likewise, the U_{out} deviations fail to stabilize, fluctuating erratically between 16.0% and 25.8%. This confirms that in the optimization process using strategy 1, acceptable results are determined primarily by chance. The obtained U_{in} values are the only ones demonstrating result convergence (1.0–1.96%), which is attributed to the imbalance of OF F_1.

The analysis of the strategy 1 results demonstrates its drawback associated with the normalization of OF F_1. Due to the use of a weighted sum of criteria and normalization relative to the $E(t)$ value, the amplitude criterion error contributed significantly less to the OF value compared to the matching criterion error. Consequently, the optimization process over-prioritized the matching criterion at the expense of identifying solutions with minimal U_{out} values.

TABLE III. MF OPTIMIZATION RESULTS FOR STRATEGY 2

№	MF ID	t, µm	h, µm	s_1, µm	s_2, µm	U_{in}, mV	U_{out}, mV
N_{it}=500							
1	N	18.0	154.0	647.6	409.8	514	53
2	H	29.6	149.0	338.7	1239.2	518	46
3	F	19.3	216.4	367.8	582.4	533	50
4	F	19.6	129.7	812.1	1329.4	521	48
5	G	26.3	135.7	378.1	1707.7	514	44
Δ, %		24.4	25.1	41.1	61.3	1.9	9.3
N_{it}=1000							
1	F	24.4	104.5	938.9	1620.4	511	48
2	H	18.4	105.5	393.6	1638.4	506	40
3	L	21.0	194.3	100.9	1250.1	507	39
4	J	27.2	191.0	162.7	854.3	502	50
5	N	21.0	122.0	1946.3	1077.5	521	48
Δ, %		19.3	30.1	90.1	31.5	1.9	12.4
N_{it}=2500							
1	G	19.8	138.5	146.6	1004.4	499	41
2	**H**	**20.3**	**142.5**	**104.0**	**1285.2**	**501**	**37**
3	G	20.5	139.2	102.1	934.4	493	41
4	H	36.8	147.4	167.9	1121.3	505	43
5	G	19.5	152.6	185.9	1153.7	509	41
Δ, %		30.7	4.8	29.1	15.8	2.0	7.5

Strategy 2 also exclusively synthesized MF 3 topological variants. However, Table III confirms that strategy 2 yields significantly lower U_{out} values and drastically improved convergence. At N_{it}=500, the best result was U_{out}=44 mV at U_{in}=514 mV (run 5, MF G), and at N_{it}=1000, the voltage decreased to U_{out}=39 mV at U_{in}=514 mV (run 3, MF L). With an increase in N_{it} to 2500, the algorithm consistently selects two MFs (MF H and MF G) as the best solutions.

The analysis of deviation Δ for the strategy 2 results reveals an important feature of the selection process. As N_{it} increases, the deviations for h and s_2 steadily decrease (to 4.8% and 15.8%, respectively). The deviation for s_1 also decreases (to 29.1%), although it remains high, similar to that for t (30.7%). Initially, this might imply that these parameters are the most sensitive to changes in OF F_2, and convergence could be achieved with a further increase in N_{it}. However, given the tight convergence of the actual criteria (Δ for U_{out} and U_{in} at N_{it}=2500 is only 7.5% and 2%, respectively), these broad parameter deviations actually stem from the algorithm identifying two distinct MF topologies that equally satisfy OF F_2. Notably, the U_{out} deviation at N_{it}=2500 is nearly 3 times smaller than in strategy 1 (7.5% compared to 20.0%). Meanwhile, U_{in} values remain within the acceptable range of 493–533 mV across all runs (the Δ for U_{in} differs from strategy 1 by only 1% at N_{it}=2500), confirming the validity of the transition to OF F_2.

A comparison of the two approaches demonstrates the evident advantage of strategy 2. Specifically, at N_{it}=1000, the U_{out} value decreases by 29% (39 mV compared to 55 mV) relative to strategy 1, and at N_{it}=2500, it decreases by 19.6% (37 mV compared to 46 mV). Thus, strategy 2 (with stepwise narrowing of the optimized parameter ranges) and OF F_2 with modified normalization coefficients significantly enhance the stability of identifying higher-quality solutions.

Crucially, across all runs, the best-synthesized topologies consistently featured broad-side electromagnetic coupling (MF 3 variants). Positioning conductors strictly opposite each other across the substrate maximizes the difference in per-unit-length mode delays which is an absolute prerequisite for effective USP decomposition.

Overall, the best result (based on the set of criteria) was demonstrated by MF H, obtained through generative synthesis and structural-parametric optimization using strategy 2 at N_{it}=2500. In this case, MF matching with the path (U_{in}=501 mV) and the lowest USP amplitude (U_{out}=37 mV) were ensured. The optimized parameters for MF H were as follows: t=20.3 µm, h=142.5 µm, s_1=104.0 µm, and s_2=1285.2 µm. A general view of the MF H cross section is shown in Fig. 4, and the waveforms of $E(t)$ and the voltages at the MF H input U_{in} and output U_{out} are presented in Fig. 5.

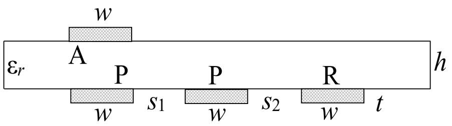

Fig. 4. Cross section of the synthesized MF H topology.

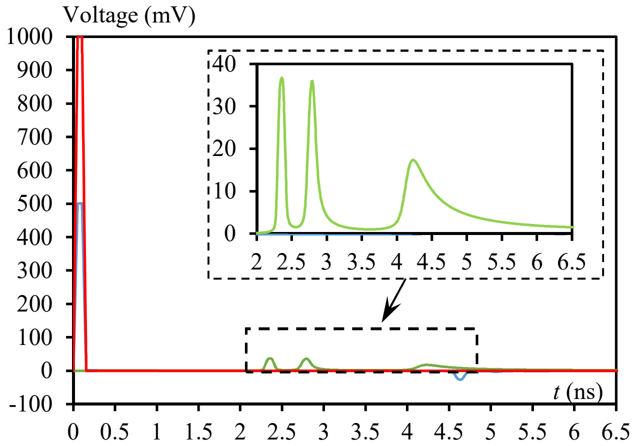

Fig. 5. $E(t)$ (—) and the voltage waveforms at the input U_{in} (—) and output U_{out} (—) of MF H obtained as a result of structural-parametric optimization using strategy 2.

Fig. 5 demonstrates the successful achievement of both optimization criteria. The input voltage U_{in} stabilizes at 501 mV, indicating near-ideal impedance matching to the transmission path. At the output, the MF clearly decomposes the incident USP into three primary pulses. The optimization successfully equalized the amplitudes of the first two pulses at a minimal 37 mV. Meanwhile, the third pulse remains significantly smaller (approximately 17 mV). While this amplitude gap hints at an untapped margin for further minimizing U_{out} by fully equalizing all three pulses, forcing such an equalization would inevitably induce impedance mismatch, directly violating the OF constraints. Ultimately, the MF H topology represents an optimal trade-off, i.e. it maximizes USP attenuation (by a factor of over 13 relative to U_{in}) while rigorously preserving the integrity of the high-frequency useful signal.

IV. Conclusion

In conclusion, these results advance the automated design of strip MFs by integrating generative template synthesis with global structural-parametric optimization. We demonstrated that relying on a traditional direct search across the entire parameter space wastes computational resources and severely risks prematurely losing the global extremum. It should be noted that the presented results are theoretical in nature and aim to confirm the computational efficiency of the proposed search strategies without being bound by strict manufacturing constraints. The transition from a continuous parameter space to a discrete one (accounting for technological fabrication standards) and the execution of experiments are scheduled for subsequent research stages.

We successfully validated the proposed search strategies, with strategy 2 proving highly effective. It synergizes the LHS algorithm with dynamic search space narrowing and a least-squares-based OF F_2, enhanced by pre-calibrated normalization coefficients. This approach not only automated the synthesis and evaluation of 14 distinct topologies but also decisively narrowed the field down to the two optimal candidates (both featuring strong broad-side coupling). These configurations maximize USP decomposition while maintaining strict impedance matching. Ultimately, the best solution attenuates the exciting USP by a factor exceeding 13.

Future research will focus on exploring alternative search strategies and hybridizing the global search with local optimization algorithms in the final stages. Furthermore, we plan to expand the generative synthesis space to incorporate multilayer MF structures, including those integrating radio-absorbing materials and alternative conductor geometries. We will also analyze the impact of cross-sectional geometric asymmetry and extend this generative methodology to cable-based MFs.

References

[1] W. A. Radasky and R. Hoad, “Recent Developments in High Power EM (HPEM) standards with emphasis on High Altitude Electromagnetic Pulse (HEMP) and Intentional Electromagnetic Interference (IEMI),” IEEE Lett. Electromagn. Compat. Pract. Appl., vol. 2, no. 3, pp. 62–66, Sept. 2020, doi: 10.1109/LEMCPA.2020.3009236.

[2] N. M’ziou, “Electromagnetic compatibility problems of indirect lightning stroke on Overhead Power Lines,” Math. Comput. Simul., vol. 167, pp. 429–442, Jun. 2020, doi: 10.1016/j.matcom.2018.04.007.

[3] J. Bai, Y. Shi and G. Zhao, “Research on electromagnetic interference of vehicle GPS navigation equipment,” 2017 IEEE 5th International Symposium on Electromagnetic Compatibility (EMC-Beijing), Beijing, China, 2017, pp. 1–5, doi: 10.1109/EMC-B.2017.8260366.

[4] N. Mora, F. Vega, G. Lugrin, F. Rachidi, and M. Rubinstein, “Study and classification of potential IEMI sources,” System design and assessment notes, Note 41, Jul. 2014, pp. 1–48.

[5] J. Zhang, C. Ning, J. Heng, S. Yu, and Z. Zhang, “Ultra-Short Pulse Generation From Optical Parametric Oscillators With a Cavity-Length Detuning,” IEEE Photon. Technol. Lett., vol. 34, no. 5, pp. 263–266, Mar. 2022, doi: 10.1109/LPT.2022.3149528.

[6] R. Gaynutdinov and S. Chermoshentsev, “Studies of Electromagnetic Disturbances in Coupling Path by Application of Intentional Ultrashort Electromagnetic Pulses,” 2019 International Conference on Electrotechnical Complexes and Systems (ICOECS), Ufa, Russia, 2019, pp. 1–4, doi: 10.1109/ICOECS46375.2019.8949973.

[7] M. G. Nuriev, R. M. Gizatullin, and Z. M. Gizatullin, “Physical Modeling of Electromagnetic Interferences in the Electronic Devices at Direct Impact of Lightning on Protection System of Building,” 2018 XIV International Scientific-Technical Conference on Actual Problems of Electronics Instrument Engineering (APEIE), Novosibirsk, Russia, 2018, pp. 355–358.

[8] A. T. Gazizov, A. M. Zabolotsky, and T. R. Gazizov, “UWB Pulse Decomposition in Simple Printed Structures,” IEEE Trans. Electromagn. Compat., vol. 58, no. 4, pp. 1136–1142, Aug. 2016, doi: 10.1109/TEMC.2016.2548783.

[9] T. R. Gazizov, A. M. Zabolotsky, and A. T. Gazizov, “Decomposition of ultra-wideband pulses in transmission lines with modal dispersion,” IEEE Trans. Electromagn. Compat., vol. 54, no. 1, pp. 160–168, Feb. 2012.

[10] A. O. Belousov et al., “From symmetry to asymmetry: the use of additional pulses to improve protection against ultrashort pulses based

on modal filtration," Symmetry, vol. 12, no. 7, p. 1117, 2020, doi: 10.3390/sym12071117.

[11] Y. S. Zhechev et al., "Routing Technique for Microwave Transmission Lines to Ensure UWB Interference Immunity," IEEE Trans. Microw. Theory Techn., vol. 71, no. 12, pp. 5304–5316, Dec. 2023, doi: 10.1109/TMTT.2023.3276029.

[12] I. P. Norenkov, Automatic design, (in Russian), Moscow, Russia: MSTU named after N. E. Bauman, 2000, 188 p.

[13] L. A. Rastrigin, Statistical search methods, (in Russian), Moscow, USSR: Nauka, 1968, 376 p.

[14] S. P. Kuksenko, "Preliminary results of TUSUR university project for design of spacecraft power distribution network: EMC simulation," IOP Conf. Ser.: Mater. Sci. Eng., vol. 560, no. 012110, pp. 1–7, 2019.

[15] J. C. Helton and F. J. Davis, "Latin hypercube sampling and the propagation of uncertainty in analyses of complex systems," Reliab. Eng. Syst. Saf., vol. 81, no. 1, pp. 23–69, Jul. 2003, doi: 10.1016/S0951-8320(03)00058-9.

[16] A. O. Belousov and V. O. Gordeeva, Optimization of interference protection structures with modal decomposition: monograph, (in Russian), Tomsk, Russia: TUSUR University Press, 2023, 136 p.